Nonlinear imaging (NIM) of flaws in a complex composite stiffened panel using a constructive nonlinear array (CNA) technique

Gian Piero Malfense Fierro and Michele Meo
University of Bath, Materials Research, Department of Mechanical Engineering, Claverton Down, Bath, UK

Abstract
Recently, there has been high interest in the capabilities of nonlinear ultrasound techniques for damage/defect detection as these techniques have been shown to be quite accurate in imaging some particular type of damage. This paper presents a Constructive Nonlinear Array (CNA) method, for the detection and imaging of material defects/damage in a complex composite stiffened panel. CNA requires the construction of an ultrasound array in a similar manner to standard phased arrays systems, which require multiple transmitting and receiving elements. The method constructively phase-match multiple captured signals at a particular position given multiple transmit positions, similar to the total focusing method (TFM) method. Unlike most of the ultrasonic linear techniques, a longer excitation signal was used to achieve a steady-state excitation at each capturing position, so that compressive and tensile stress at defect/crack locations increases the likelihood of the generation of nonlinear elastic waves. Moreover, the technique allows the reduction of instrumentation nonlinear wave generation by relying on signal attenuation to naturally filter these errors. Experimental tests were carried out on a stiffened panel with manufacturing defects. Standard industrial linear ultrasonic test were carried out for comparison. The proposed new method allows to image damages/defects in a reliable and reproducible manner and overcomes some of the main limitations of nonlinear ultrasound techniques. In particular, the effectiveness and robustness of CNA and the advantages over linear ultrasonic were clearly demonstrated allowing a better resolution and imaging of complex and realistic flaws.

Keywords: Nonlinear Ultrasound, Phased Array, Laser Vibrometer, TFM, Composite

1. Introduction

Over the last sixty years NDT/E has been an area of continued growth, the need for such methods has increased dramatically in recent years due to the need for [1]: product safety, in-line diagnostics, quality control, health monitoring, security testing, etc. Over the last two decades due to the high cost of inspection of composite materials compared with metallic structures, development of a reliable and effective NDT/E method to detect the occurrence of critical failure modes in composites has been pursued [2-5].
Currently there are various NDT/E techniques that are available for material evaluation, these methods although essential for the testing of materials are not without drawbacks, which include: time, cost and defect discovery concerns. One of the most promising and well-developed fields of NDT/E is ultrasonic testing methods which have been found to provide high levels of suitability and effectiveness in damage/defect evaluation and have become very popular due to their capability, flexibility and relative cost-effectiveness.
Ultrasonic testing can be broadly defined into two groups those based on principles of linear ultrasound and those based on principles of nonlinear ultrasound. Linear ultrasound methods include reflection, transmission, mode-conversion, scattering and absorption of acoustic energy caused by a defect [6-9]. Nonlinear acoustics include harmonic generation, frequency mixing and modulation of ultrasound by low-frequency vibration [10-12]. While linear techniques identify cracks by detecting the amplitude and/or phase change of the response signal caused by defects when a consistent probe signal is applied, nonlinear techniques correlate defects with the presence of additional frequency components in the output signal [13]. The current shift away from linear ultrasonic techniques is mainly due to the fact that the sensitivity of nonlinear methods to study damage evolution appears to be a few orders of

magnitude higher , while linear techniques are only sensitive to gross defects rather than micro-damage [14].

One of the main issues that has restrained the adoption of nonlinear ultrasound techniques in industry has been the repeatability and effectiveness of these techniques, as the frequency dependence of these techniques makes it difficult to determine which excitation frequency to use. Works by Solodov *et al* propose a solution based on the resonant ultrasonic wave-defect interaction due to local defect resonance (LDR) [15-17]. LDR is determined by known geometry, material characteristics and boundary conditions, results have shown a strong increase in vibration amplitude at these frequencies. One of the issues with such methods is that they rely on known damage location and material properties, without prior knowledge of damage location it becomes difficult to determine the frequency of LDR. This work proposes a method focused on material resonance determined by forced ultrasound excitation, where damage location and material properties are unknown.

Ultrasonic phased array techniques arguably lead the field in terms of damage detection capabilities and suitability for composite material structures. Phased array systems generally use an array of transmitting and receiving piezoelectric elements, where the sequence of firing and capturing determines the method and accuracy. These systems generally use three methods for damage assessment and imaging, such as the plane/focus swept method, full matrix capture (FMC) and total focusing method (TFM) a post-process technique [18, 19].
The geometry of a general phased array is highlighted in Figure 1, while Figure 2 presents the various techniques available. These B-scan techniques can then be performed along the surface of the structure (y-axis) in order to generate a C-scan image.

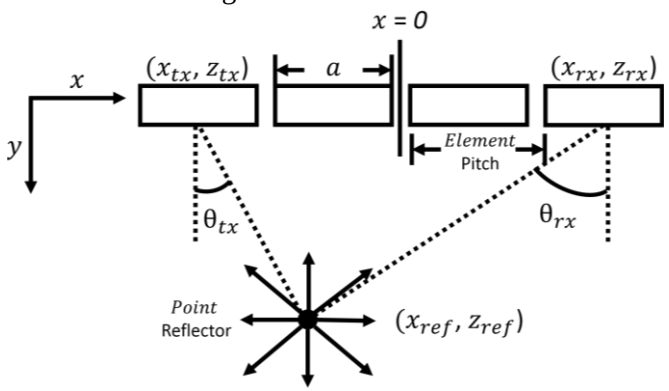

Figure 1: Phased array geometry

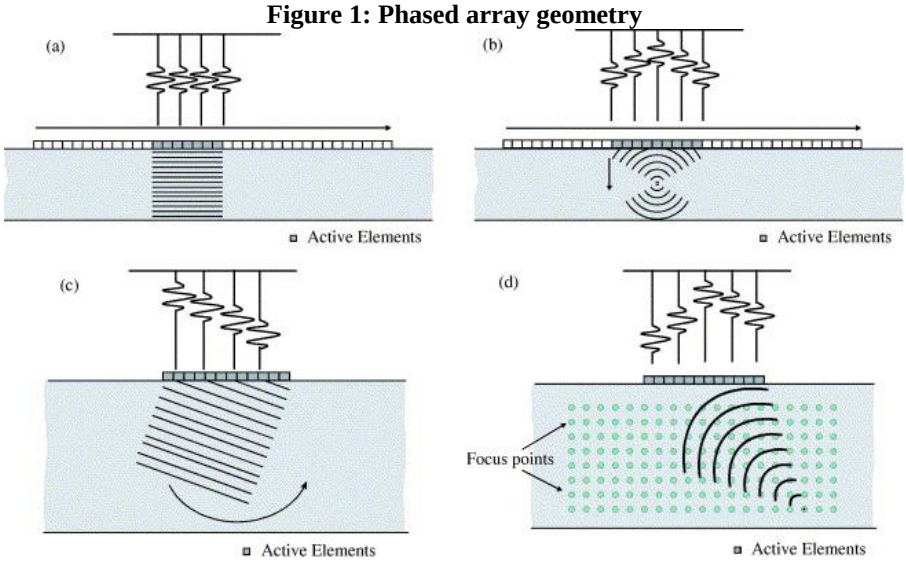

Figure 2: Schematic diagram of the (a) plane swept B-scan, (b) focused swept B-scan, (c) sector B-scan and (d) fully focused TFM, image from [20].

The TFM method uses a post-processing algorithm which discretises the thickness of a sample into a grid (as shown in the figure above (d)). The signals from all the elements in the array (referring to that grid point) are then summed to focus at every point in the grid. The intensity of the image, $I(x,z)$ at any point in the scan is given by:

$$I(x,z)=\left|\sum h_{tx,rx}\left(\frac{\sqrt{(x_{tx}-x)^2+z^2}+\sqrt{(x_{rx}-x)+z^2}}{c_1}\right)\right| \quad (1)$$

$$summed \;\; for \;\; \left|x_{tx,rx}-x\right|\leq\frac{D}{2}s$$

where: D is the width of the aperture, z and x are distances in z-direction (normal to array, depth) and x-direction (position along array) for transmitting (*tx*) and receiving elements (*rx*) (Figure 1), $h_{tx,rx}$ is the Hilbert transform of the time domain signal, c_1 is the speed of sound in the medium, *s* is the step along the array which sets the resolution of the B-scan.

Nonlinear ultrasound phased array techniques have been assessed by the following authors [21-28]. Ohara *et al* and Park *et al* have extensively developed and evaluated and improved the detection of open and closed cracks in metallic structures using a subharmonic phased array, while Potter *et al* has developed a nonlinear array based on the traditional TFM. These methods provide nonlinear ultrasound information through the thickness of the sample, rely on short excitation signals, have been assessed on metallic structures and do not generally address issues of equipment based nonlinearities.

A constructive nonlinear array (CNA) technique is proposed for optimum nonlinear imaging (NIM) of difficult flaws in laminated structures. Specifically, CNA is a post-process technique (but not limited to this) used to constructively phase match multiple captured signals at a particular position (*k*) given multiple transmit positions (*j*), similar to the TFM method. This is done by capturing the signal on the surface of the structure using a laser vibrometer (LV) and exciting from multiple locations. The technique phase matches continuous time domain signals in order to ensure constructive interference in a specific location, which is unlike the TFM method that uses short pulses and post-process beam focusing to generate grid intensity values. This longer signal (captured using CNA) provides more information with regards to the frequency spectrum of the signal (unlike pulses that have low frequency resolution), essential for accurate nonlinear ultrasound methods which rely on frequency domain components (harmonics). An added benefit of longer excitation is that it ensures that steady-state excitation is achieved at the capturing position, this results in a prolonged ultrasonic force acting on damaged/defected regions and ultimately increasing the likelihood of the generation and capture of nonlinearities from these regions.
CNA relies on the capturing of each received signal independently for each transmitting position, which has similarities with various linear and nonlinear ultrasound phased array techniques. Although, unlike linear and nonlinear techniques, which use phase shifts (time lags) between signals in the time domain to focus on individual points through the thickness of a medium, this methods looks to aggregate in-phase time signals in order to focus on the nonlinear content of the signal in the frequency domain.

The CNA method has been used to evaluate a defect region which was located in a difficult accessibility, the radii of a composite T-Section. Various linear phased array techniques have been developed to test pieces of complex geometry [29-34]. These methods have focused on numerical simulation and the development of corner-shaped components and smart flexible arrays. The main short-comings of these proposed methods is that, although detection is possible using these methods, they require direct measurement (‘line-of-sight’) over the damage region. Furthermore on more complex structures and

fixed assemblies it may not be possible to position these probes or wedges. The proposed CNA method does not require direct measurement over the defect region, but rather steady-state excitation of the damage region as it depends on the propagation of nonlinearities from these locations which has been shown in the results.

Nonlinearities produced by equipment errors and instabilities are a great concern for nonlinear techniques, as the amplitudes of further harmonics are generally small and thus can be greatly altered by these effects. Further to this, small damages/defects generally require large excitation amplitudes in order for nonlinearities to generate and propagate from these regions, it is well known that the amplification of ultrasound signals result in an increase of equipment based nonlinearities, due to amplifiers and waveform generators. Thus, there is a trade-off between the excitation amplitude used for damage detection and the capability of these methods to accurately detect damage.
CNA proposed here relies on the propagation of waves throughout a structure and generally over large relative distances when compared with through thickness phased array techniques. This means that due to frequency attenuation unwanted equipment harmonics will tend to zero as distance increases, the method suggests that given a high number of transmit positions these effects will reduce and eventually become redundant, vastly improving the potential of nonlinear ultrasonic imaging techniques. Thus the CNA method provides a 'natural filter' against unwanted equipment based harmonics.
The effectiveness of CNA was evaluated using a T-section stiffened composite panel with embedded damaged (Teflon strip). A LV was used to capture time domain signals located over a grid of positions on the surface of the flange and either side of the web. The methodology will be discussed in more detail in the next sections. CNA was used to evaluate five nonlinear parameters: β (related to the second harmonic, A_2); γ (A_3); δ (A_4); ε (A_5) and A_{Half} ($A_{1/2}$), refer to equation (4). The result clearly show the ability of CNA to determine the damage location as well as how constructive interference and frequency attenuation provide cleaner images that outperformed the fundamental frequencies results.

2. Nonlinear Ultrasound Theory

Nonlinear elastic wave spectroscopy (NEWS) techniques have been shown to be innovative ultrasonic NDE and SHM inspection methods. Some of these methods centre on the theory of 'clapping/rubbing mechanism' (such as defects and damages), which generate nonlinear elastic effects which can be evaluated using the frequency response of a time domain signal [35]. Compared to linear ultrasound methods, these techniques have shown higher sensitivity in diagnosing material micro-defects such as porosity, inclusions and early stage damage in the form of micro-cracks, delaminations and adhesive bond weakening [5, 14, 35-40].
These nonlinear elastic effects give rise to further harmonic responses known as the second, third and fourth harmonics (and so forth). It has also been shown that subharmonic production can also be produced by such mechanisms which also provide higher sensitivity than linear ultrasound techniques [41-43]. Nonlinear ultrasound uses these extra harmonics to determine the extent of defects in a material. Figure 3 highlights the potential frequency response spectrum:

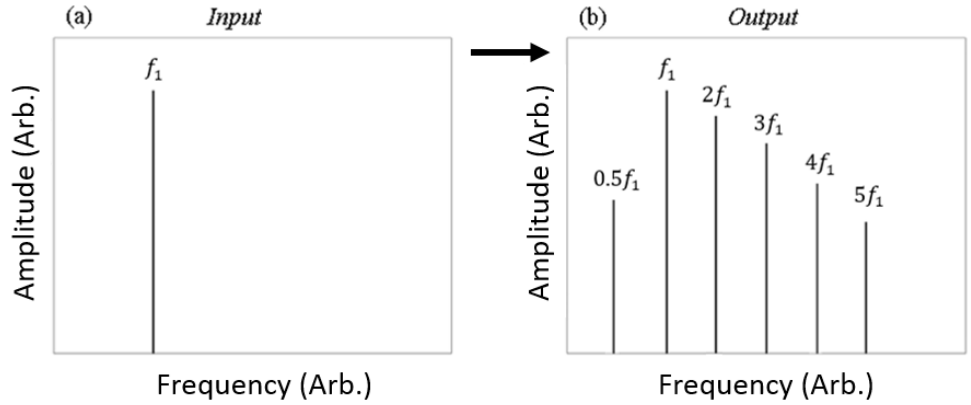

Figure 3: Plot (a) shows the input signal for a single frequency, plot (b) shows the output signals for a single frequency.

The fundamental equations used and developed in order to determine the further harmonics (second and third order nonlinearity parameters) are highlighted below. The second order nonlinearity parameter (β_p) can be described by the equation below. [44]:

$$\beta_p = \frac{8A_2}{A_1^2 k^2 a_1} \tag{2}$$

Where: A_1 and A_2 are the respective frequency amplitudes of the first and second harmonics of the recorded time domain waveforms, *k* is the wavenumber, and a_1 is the propagation distance. The second and third order nonlinearity parameter (γ_p) allows for experimental evaluation of the respective nonlinear parameter, the third order parameter is shown below [45]:

$$\gamma_p \approx \frac{A_3}{A_1}\frac{48}{k^3 a_1} \tag{3}$$

where: A_3 is the frequency amplitude of the third harmonic of the recorded time domain waveform.

The simplified nonlinearity parameters considered in this piece of work are as follows:

$$\beta_P \approx \beta \approx \frac{A_2}{A_1}; \quad \gamma_P \approx \gamma \approx \frac{A_3}{A_1}; \quad \delta \approx \frac{A_4}{A_1}; \qquad \varepsilon \approx \frac{A_5}{A_1}; \qquad A_{Half} \approx \frac{A_{1/2}}{A_1}; \tag{4}$$

where: A_4 is the amplitude of the 4th harmonic ($4f_1$), A_5 is the amplitude of the 5th harmonic ($5f_1$), $A_{1/2}$ is the amplitude of the subharmonic ($0.5f_1$).

Phase matching and the constructive interference methodology proposed in the next section is intended to be used on the fundamental frequency as well as matching the nonlinear responses ($f_1, 2f_1, 3f_1, 4f_1, 5f_1, f_{1/2}$), i.e. frequency selective constructive interference. For example: in order to constructively match the second harmonic, all time signals are shifted with respect to A_2 not A_1 and the following is true for all subsequent harmonics.

3. Theory and Background

3.1. Phase Matching and Constructive Interference

Considering an array with transmitting position *j* and receiving element *k* (Figure 4) the time domain signal with a certain frequency (*f*) can be represented as $f_{j,k}(t)$, thus the sum of all the transmitting elements at receiving position *k* can be defined by the below equation:

$$f_k(t) = \sum_{j=1}^{\infty} f_{j,k}(t) \tag{5}$$

When considering multiple locations for j with a constant position k, a solution to get the maximum information in the receiving element k is to match the phase of $f_{j,k}(t)$ and $f_{j+1,k}(t)$ to obtain a constructive interference (when exciting from multiple (j) positions at the same time).

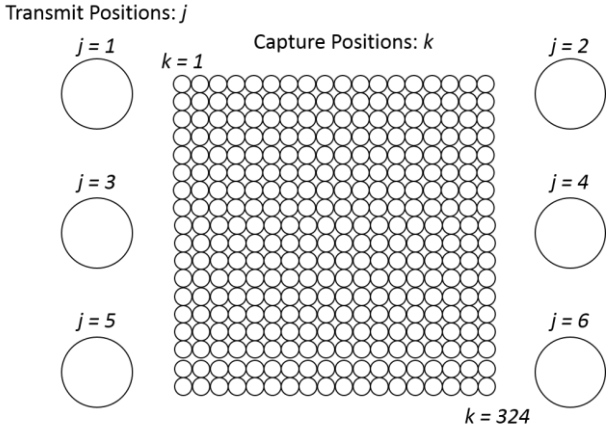

Figure 4: Example of transmit positions (j) and capturing positions (k)

Considering two transducer positions 1 and 2, phase matching between two captured signals at position k for a frequency of F can be achieved by determining:

$$F_{2,k} = \max\left(\left\{\int_0^T abs\left(\left(f_{1,k}(t) + f_{2,k}(t+\Delta t_1)\right)\right)dt, \ldots, \int_0^T abs\left(\left(f_{1,k}(t) + f_{2,k}(t+\Delta t_n)\right)\right)dt\right\}\right) \tag{6}$$

Equation 6 solves for the maximum constructive interference between the two signals, phase matching the two signals and providing a max amplitude at point k. Figure 5 shows how constructive and destructive interference affects the amplitude of two summed signals with a frequency (f) as a function of Δt_n (phase lag). Maximum constructive interference occurs within one period shift (T_p, time to complete n periods calculated by $n.(1/f)$ with n=0,1,2…) of two signals with a total time (T), assuming a frequency of f.

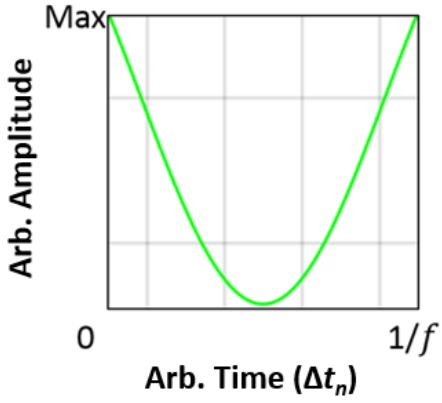

Figure 5: Constructive vs. Destructive Interference

Based on this, equation 6 becomes:

$$F_{2,k} = \max_{i \in [n]}\left(\left\{\int_0^T abs\left(\left[f_{1,k}(t) + f_{2,k}(t+\Delta t_i)\right]\right)dt\right\}\right) \tag{7}$$

$$[n] = \{1, \ldots, (T_P / t_{step} + 1)\} \tag{8}$$

where: Δt is the time shift applied to the signal, and n refers to the number of shifts in time required to satisfy the condition. The value of Δt is defined by:

$$\Delta t_i = \left\lfloor i \times t_{step} - t_{step} \right\rfloor \tag{9}$$

$$t_{step} = \frac{1}{f_s} \tag{10}$$

Given a signal captured using a specific sampling frequency (f_s) the minimum shift in the time step is given by t_{step} and thus the maximum resolution in obtaining constructive interference is limited to this value, unless interpolation of each time signal is done. The procedure can be repeated if multiple array transmit positions (P) are considered: phase matching for all subsequent transmit positions can be done by finding Δt the time shift required to meet the max constructive interference between transmitting element j (2 and greater, solved by considering equations 6 and 7) and the preceding constructed signal (at P-1). The procedure for a two signal system this can be expressed by:

$$F_{2,k} = f_{1,k}(t) + f_{2,k}(t + \Delta t_2) \tag{11}$$

where: Δt_2 is the time step required to maximise $F_{2,k}$, solved in equation 7. Repeating this process for all signals phase matched to j ($P \geq 2$), the constructive interference time signal is:

$$F_{P,k} = F_{P-1} + f_{P,k}(t + \Delta t_P) \tag{12}$$

where: Δt_P is the last time step shift required to maximise F_P.

This method is clearly equivalent to adding all harmonic components gathered from the fast Fourier transform of each P transmitted signal given a location k for all the transmitter combination.

3.2. Alleviation of equipment produced nonlinearities

Nonlinearities produced by equipment are well-known issues facing the accuracy of nonlinear techniques, a technique is suggested to alleviate these issues. The method focuses on the attenuation of ultrasound in a medium and uses this phenomenon to reduce equipment nonlinearities in an array setup. If we consider the fast Fourier transform of $F_{P,k}$ (equation 12), and consider the amplitudes of the fundamental (excitation frequency ($A_{1,j,k}$)) and the nonlinear responses (2nd ($A_{2,j,k}$), 3rd ($A_{3,j,k}$), 4th ($A_{4,j,k}$), 5th ($A_{5,j,k}$) and Half ($A_{1/2,j,k}$) harmonics) recorded is used to evaluate the presence of damages. If we assume that each nonlinear harmonic amplitude can be made up of equipment generated harmonics ($A_{h,j,k,equip}$) and/or damage generated harmonics ($A_{h,j,k,dam}$), the amplitude of the total nonlinear response (for harmonic h) can be defined by:

$$A_{h,j,k} = A_{h,j,k,equip} + A_{h,j,k,dam} \tag{13}$$
$$[h] = \{1/2, 2, 3, 4, 5\}$$

For a position (k) with a random material condition (either damaged or undamaged) the total nonlinear harmonic response ($H_{h,k}$) can be defined as:

$$H_{h,k} = H_{h,k,dam} + H_{h,k,equip} = \sum_{j=1}^{P} A_{h,j,k} = \sum_{j=1}^{P} A_{h,j,k,equip} + \sum_{j=1}^{P} A_{h,j,k,dam} \tag{14}$$

where: $H_{h,k,dam}$ will equal zero for an undamaged material position, $H_{h,k}$ is the total nonlinear harmonic response given by the amplitude of the fast Fourier transform of the constructively added phased matched time domain signal ($F_{P,k}$, equation 12) for a total number of transmit positions (P). The nonlinearities generated by the instrumentation decay with the distance as the material attenuates the propagating signal. The amplitude decay A_h of an ultrasound signal can be represented by the standard equations:

$$A_h\left(d_{j,k}\right) = A_0 e^{-\mu_a . d_{j,k}} \tag{15}$$

Thus an attenuation coefficient can be determined given the amplitude reduction of the signal (equation 16, below). Moreover higher frequencies attenuate more, which results in these signals not propagating as far as lower frequencies given the same material (refer to equation 18):

$$\alpha = 20\log_{10}\left(\frac{A_h\left(d_{j,k}\right)}{A_0}\right).\mu_a \tag{16}$$

$$\alpha = af^b \tag{17}$$

where: $d_{j,k}$ is the distance of propagation, A_0 is the amplitude of the signal at source, μ_a is the amplitude attenuation factor, α is the attenuation coefficient, a is the attenuation given a specific frequency f (where *b* is dependent on material), it should be noted that as frequency increases so does attenuation.

Referring to equation 13 and 16, equipment generated nonlinearities ($A_{h,j,k,equip}$) emitted from transducer source P1 decays as shown in Figure 6 (b) to zero at a distance of greater than or equal to $d_{j,k,A_{h,equip}=0}$ from the source of excitation. If this position is an undamaged position (UD), which means $A_{h,j,k,dam} = 0$ and no equipment nonlinearities propagate further than this distance, hence $A_{h,j,k,equip} = 0$.

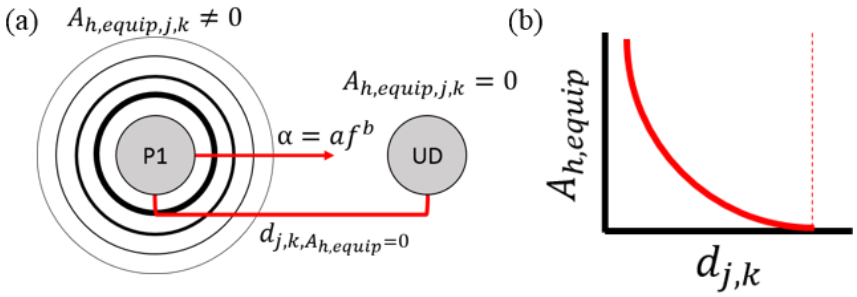

Figure 6: Decay of ultrasound signal

An example is shown in Figure 7, where four transmitter positions *j* are considered and the amplitude of the nonlinear signal is evaluate at one receiving position *k*, with *k* located at either an undamaged (UD) or damaged (D) material region. Considering the constructive phase matched time signal $F_{P,k}$ (refer to equation 12), the effect of $A_{h,j,k,equip}$ on $A_{h,j,k}$ can be evaluated with the procedure explained below. As shown in the example an array of four transmitting transducers (*j*=1 to 4, thus *P*=4) is assumed, and the receiver *k* is located at a distance ($d_{j,k,A_h=0}$) for *j*=2, 3 and 4 where the amplitude of the nonlinear wave generated by equipment decays, hence; $A_{h,j,k,equip} = 0$ (for *j*=2, 3 and 4). For *j*=1, equipment harmonics are produced at position *k* as the distance $d_{j,k,A_h\neq 0}$ falls in a location where equipment based nonlinearities have not fully decayed, thus in the below setup there is only one transducer location that contributes to equipment nonlinearities when capturing at position *k*.

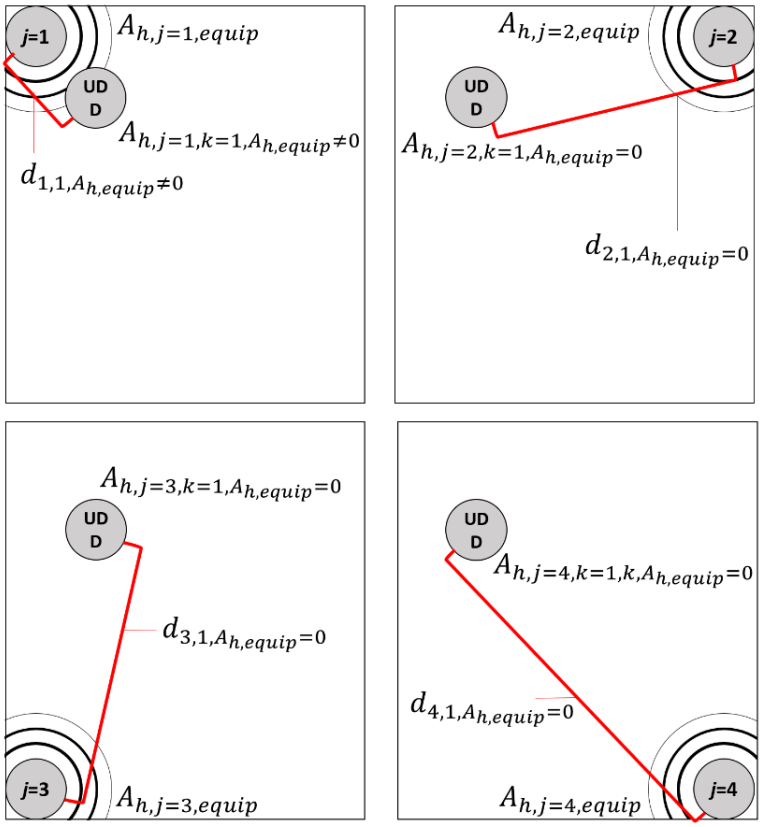

Figure 7: Undamaged Point (UD)

If the receiver *k* is located in an undamaged (UD) region, the total nonlinear harmonic response $H_{h,k,UD}$ can be evaluated as the sum of all nonlinear amplitudes captured at point *k* for each of the transmit positions:

$$H_{h,k,UD} = A_{h,j=1,k=1,equip} \tag{18}$$

As there is no nonlinear responses generated by damaged regions and the only equipment nonlinear harmonics are generated at $A_{h,j=1,k=1}$, the amplitudes captured at *k* for transmit positions *j*=2, 3 and 4 will equal zero($A_{h,j=2,k=1,equip}, A_{h,j=3,k=1,equip}, A_{h,j=4,k=1,equip} = 0$). Now if the same process is used for a damaged (D) location *k*, the sum of all nonlinear amplitudes for this condition ($H_{h,k,D}$) equals:

$$H_{h,k,D} = A_{h,j=1,k=1,equip} + A_{h,j=1,k=1,dam} + A_{h,j=2,k=1,dam} + A_{h,j=3,k=1,dam} + A_{h,j=4,k=1,dam} \tag{19}$$

In order to evaluate the total equipment generated nonlinearities ($H_{h,k,equip}$) given the array layout in Figure 7, for a position *k* of unknown damage condition (either damaged or not) the percent of equipment nonlinearities versus damage can be expressed by:

$$CH_{h,j,k,D} = \frac{H_{h,k,D,equip}}{H_{h,j,k,D}} \tag{20}$$

Now if the equipment generated nonlinearities are estimated for an extended system of infinite transmit positions *j* with damage at point *k*, the percentage contribution defined as $CH_{h,j,k,D}$ of equipment nonlinearities $H_{h,k,D,equip}$ can be expressed by the following equation:

$$CH_{h,j,k,D} = \frac{A_{h,j=1,k=1,equip}}{H_{h,j,k,D}} \tag{21}$$

Equation 21 above shows that equipment nonlinearities as a percentage contribution ($CH_{h,j,k,D}$) tend reduce as the number of transmit positions *j* are increased. In reality, the equipment produced

nonlinearities are highly dependent on $d_{j,k}$ and using a very large number of transmit positions is not possible, nor is it reasonable to expect that all except one *k* positions satisfy $d_{j,k,A_{h,k,equip}=0}$. Thus it can be assumed given a large number of transmit positions (*P*=*m*) that the equipment harmonic production as a percentage will tend to a minimum level (L, equation 22), which is a very small portion of the total harmonic amplitude captured:

$$\lim_{j \to m} CH_{h,k,D} = L \tag{22}$$

Given equation 22, the effect of equipment based nonlinearities in an array system with a large number of transmit positions (*j*) are very small when compared with nonlinearities generated by damaged regions, since:

$$\sum_{j=1}^{m} A_{h,j,k,equip} << \sum_{j=1}^{m} A_{h,j,k,dam} \tag{23}$$

$$H_{h,k,UD} < H_{h,k,D} \tag{24}$$

Now given a system with unknown damage and nonlinearities captured for each position (*k*), $H_{h,k}$ can be used to determine the nonlinear parameters (outlined in equation 4). Thus by plotting each nonlinear parameter (equation 25, below) for each position *k* in the grid, a nonlinear image can be generated and used to assess material damage.

$$\beta_k = \frac{H_{2,k}}{H_{1,k}} \qquad \gamma_k = \frac{H_{3,k}}{H_{1,k}} \qquad \delta_k = \frac{H_{4,k}}{H_{1,k}} \qquad \varepsilon_k = \frac{H_{5,k}}{H_{1,k}} \qquad A_{Half} = \frac{H_{1/2,k}}{H_{1,k}} \tag{25}$$

4. Equipment and Experimental Setup

The proposed methodology was tested on a large composite stiffened panel (CFRP: 830mm by 480mm, with a thickness of 7mm, refer to Figure 10), manufactured with a 5mm wide Teflon strip embedded down the right side of the t-section. The t-section flange had a width of 80mm, thickness of 5mm, web length of 75mm and total length of 650mm. The sample has been supplied with unknown characteristics (composite layers, thickness of layer and composite properties).

Due to the radius location of the inclusion it is very difficult to evaluate. Various techniques such as through transmission ultrasound (TTU) and various phased array techniques (plane C-scan, focused C-scan and section-scan) were used and failed to detect the defect, due to its location and rotation (refer to Figure 8 below). The TTU method evaluated the sample using various excitation frequencies using pitch/catch. The phased array techniques used a 5MHz 128 element probe using a half-step in pulse-echo evaluating both amplitude and TOF.

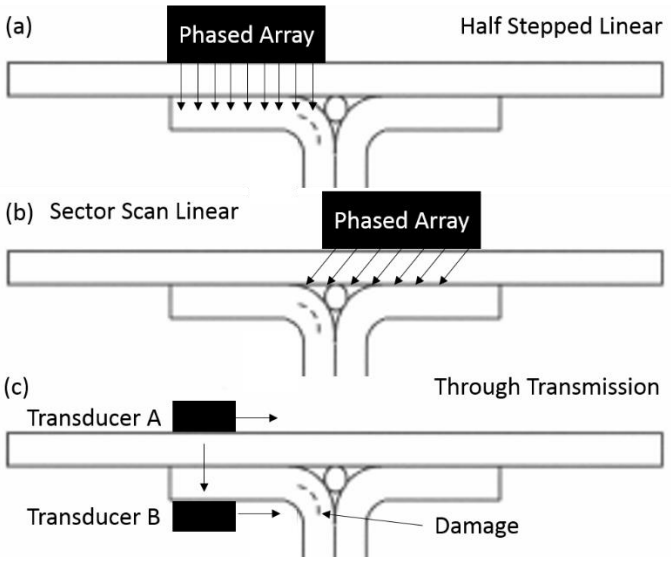

Figure 8: (a) Half-Step Linear Phased array, (b) Sector Scan Linear Phased array and (c) through transmission ultrasound (TTU)

A single frequency sinusoidal continuous wave form was generated and used to excite the damage regions. Nonlinear resonance frequency testing was used to evaluate which frequencies generated the largest second harmonic response in the material. Sweeps were conducted at intervals of 20kHz (i.e. from 20kHz to 40kHz) between 20kHz and 80kHz from the six transducer transmit location used in the final testing. An example of the process is highlighted in Figure 9 below for three transducer locations A, B and C, with one capturing position A (a position *k* in the capturing array). The green frequency response in Figure 9 refers to the response of the signal generated while the blue frequency response refers to the material response. The vertical colour coded lines refer to the maximum nonlinear responses for the second harmonic. The vertical lines also highlight the corresponding fundamental and third harmonic responses. It is clear to see that the maximum nonlinear response does not always relate to the maximum fundamental response, and that the material response (in this case a local resonance) is dependent on excitation location and capturing position, which is expected. In this instance the capturing position was located on either side of the T-Section in-line with the transducer location (refer to Figure 11). Excitation frequency was chosen according to which frequency gave the largest nonlinear response and whether a similar response was found at the other transmit locations. In the example in Figure 9, a frequency of f2 would be selected and used as it resulted in large nonlinear responses in all locations tested. As it is unlikely to find the same frequencies in all transmit location it, the frequency that is most common in the transmit locations should be used. This process was conducted for the tested sample with a frequency of 28.3kHz being selected for CNA evaluation.

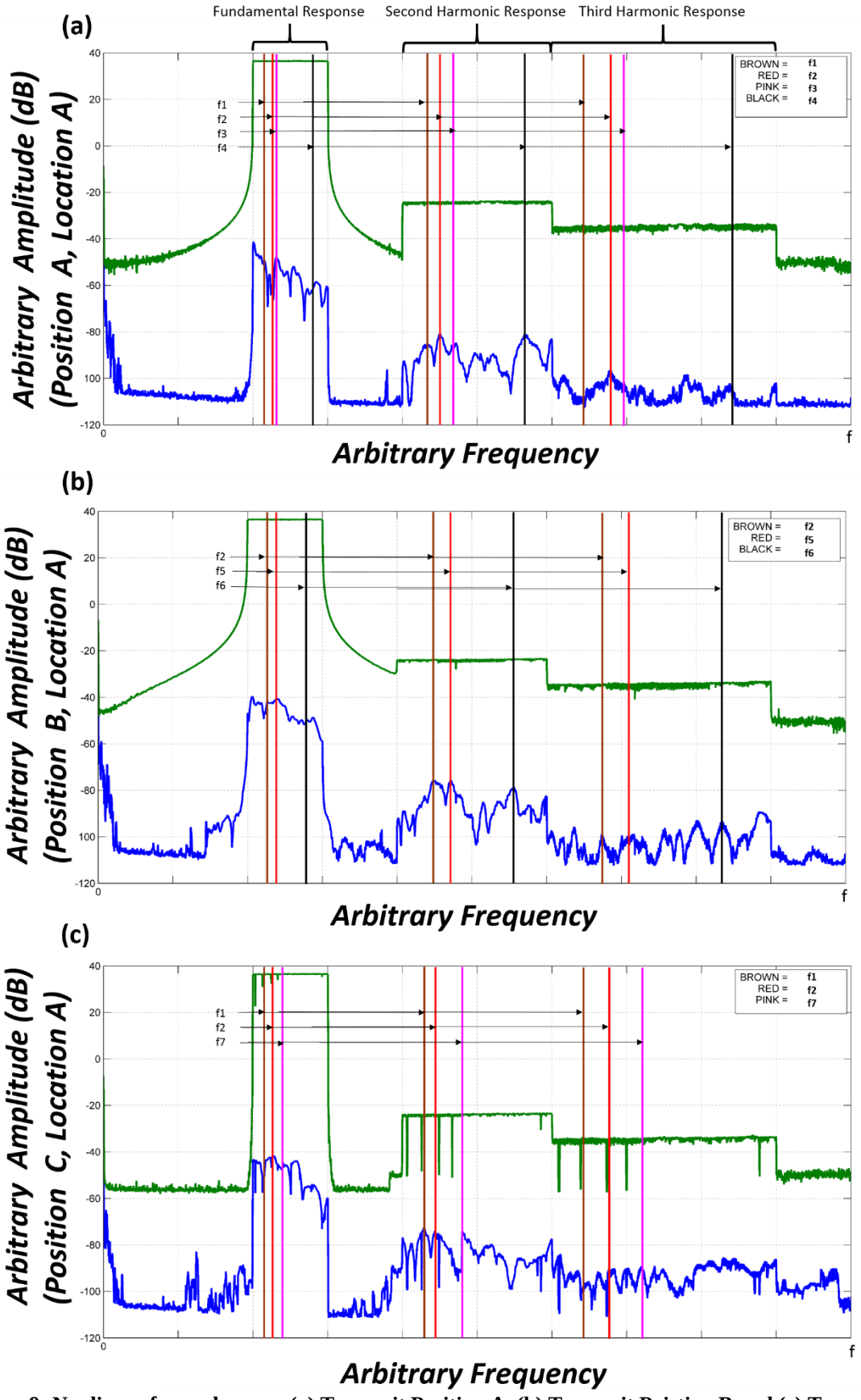

Figure 9: Nonlinear focused sweep, (a) Transmit Position A, (b) Transmit Poistion B and (c) Transmit Position C

Figure 10 (a) shows the full panel that was used during testing with the inspected area highlighted with a green dotted box, this has been enlarged in Figure 10 (b) to show the LV grid points captured and damage location. In Figure 10 (c) the cross-section of the T-Section is shown in detail with relevant measurements. Figure 11 (a), like in Figure 10 (a), shows the full sample with the green dotted box highlighting the area shown in Figure 11 (b). Figure 11 (b) shows the general layout of the experiment with transmitting locations superimposed onto the image (P1 to P6) as well as the damage location shown as a red line.

The input signals were generated using a function generator (built in generator - Polytec PSV-A-420) linked to an amplifier (Falco Systems, DC to 5 MHz, High Voltage WMA-300, x50 gain up to 300V), and applied to the structure at 200V with a piezoelectric active transducer (Piezoshaker PS-X-03-6/1000, central frequency of 60kHz). The piezoelectric active transducer had a built in suction cup and was attached with the aid of a pump, with contact aided using ultrasound coupling gel. The direct out-of-plane vibration responses were captured and averaged 15 times using a highly sensitive LV (Polytec PSV-A-420) with two grids of 795 points (15x53, pitch between points ~1.15mm, receiving positions *k*, Figure 10). The grid covered an area on either side of the T-Section (Figure 10 and Figure 11). The signal response at each grid location (*k*) was measured with a sampling frequency of 1 MHz. Only one transducer was used to conduct the tests, this was done by moving the transmit position from *P*=1 to 6.

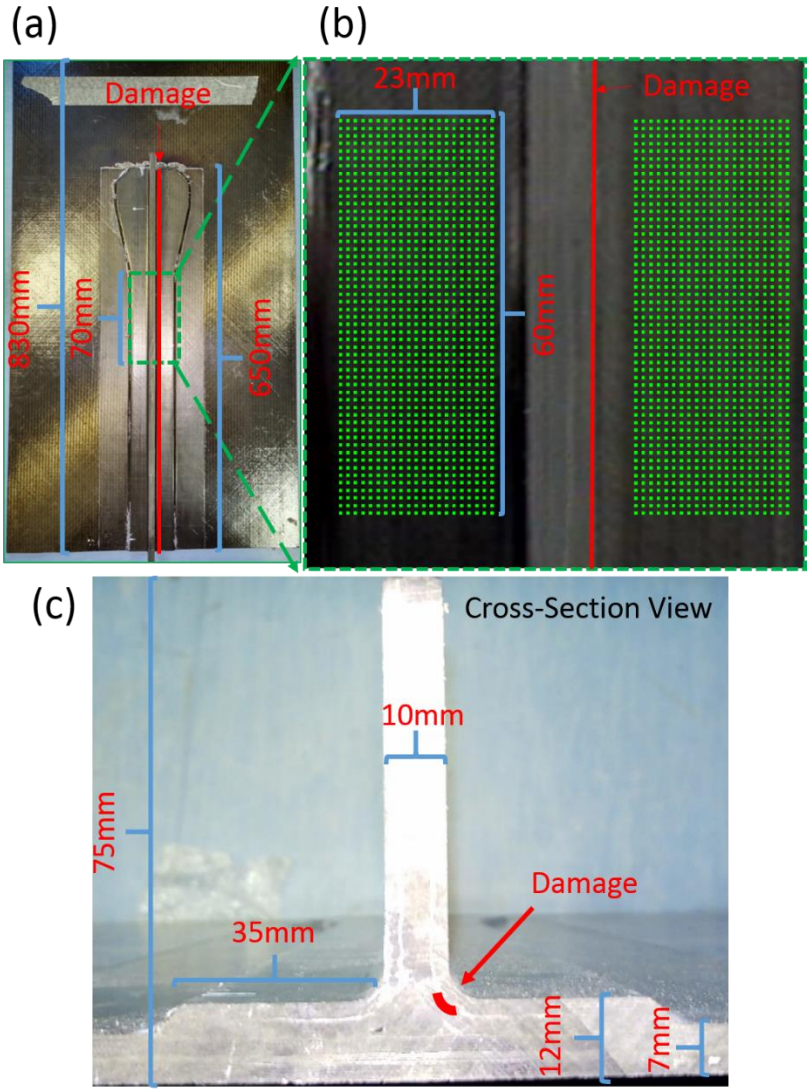

Figure 10: Composite Stiffened Panel Layout and Test Location, (a) Full Panel, (b) Zoomed Inspection Area with LV points, (c) Cross-Section View and Damage location

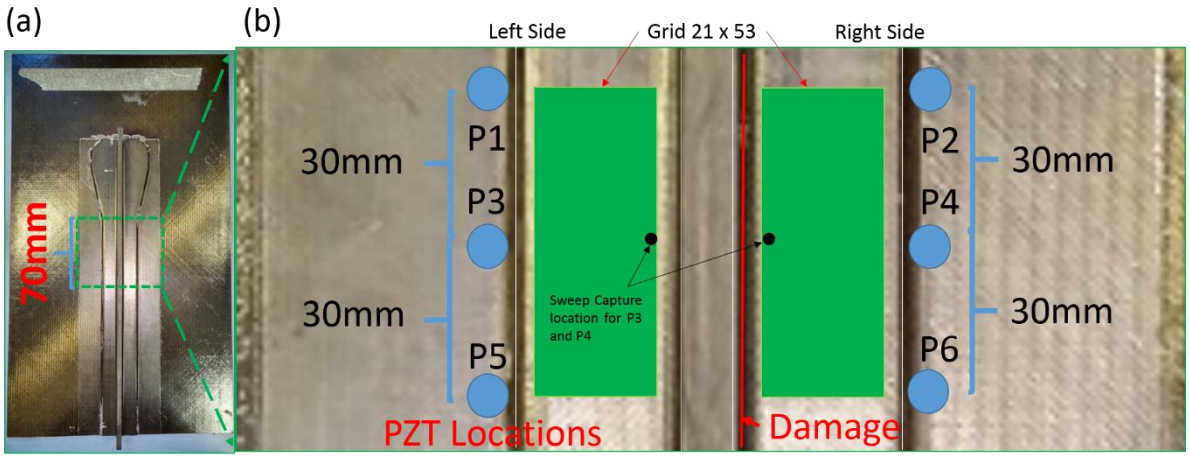

Figure 11: Experimental Setup, (a) Full Panel, (b) Zoomed Inspection Area including transmit transducer location and LV inspection area

Using the CNA technique (equation 12), $F_{P,k}$ can be experimentally determined for a given number of transmit locations *P*. Figure 12 shows how additional captured signals are used to construct the final time domain signal, in this case the fundamental frequency is considered. If the LV signal captured at a single point on the grid is considered (point 700, Figure 12 (a) and (b)) and if a maximum of 6 transmit positions is used, the constructed waveform can be generated. Figure 12 (a) shows three waveforms of varying amplitude with the smallest (orange) relating to the individual signal captured at point 700 when exciting at *j*=5, the second largest amplitude (green) corresponds to the summed phased matched signal for transmit positions 1 to 4 (i.e $F_{4,k}$, *P*=4), with the largest (yellow) relating to the phased matched sum of transmit positions 1 to 5 (i.e. $F_{5,k}$, *P*=5). Figure 12 (b) shows three waveforms in the same manner as Figure 12 (a), although they relate to the sixth transmit position (orange), $F_{5,k}$ (green) and $F_{6,k}$ (yellow). The below figure shows how the signal is constructed as transmit positions are added to the array setup, how the signal increases in amplitude and the effect that the transmit position can have on amplitude (there is a larger amplitude at point 700 when transmitting from *j*=4 than *j*=5).

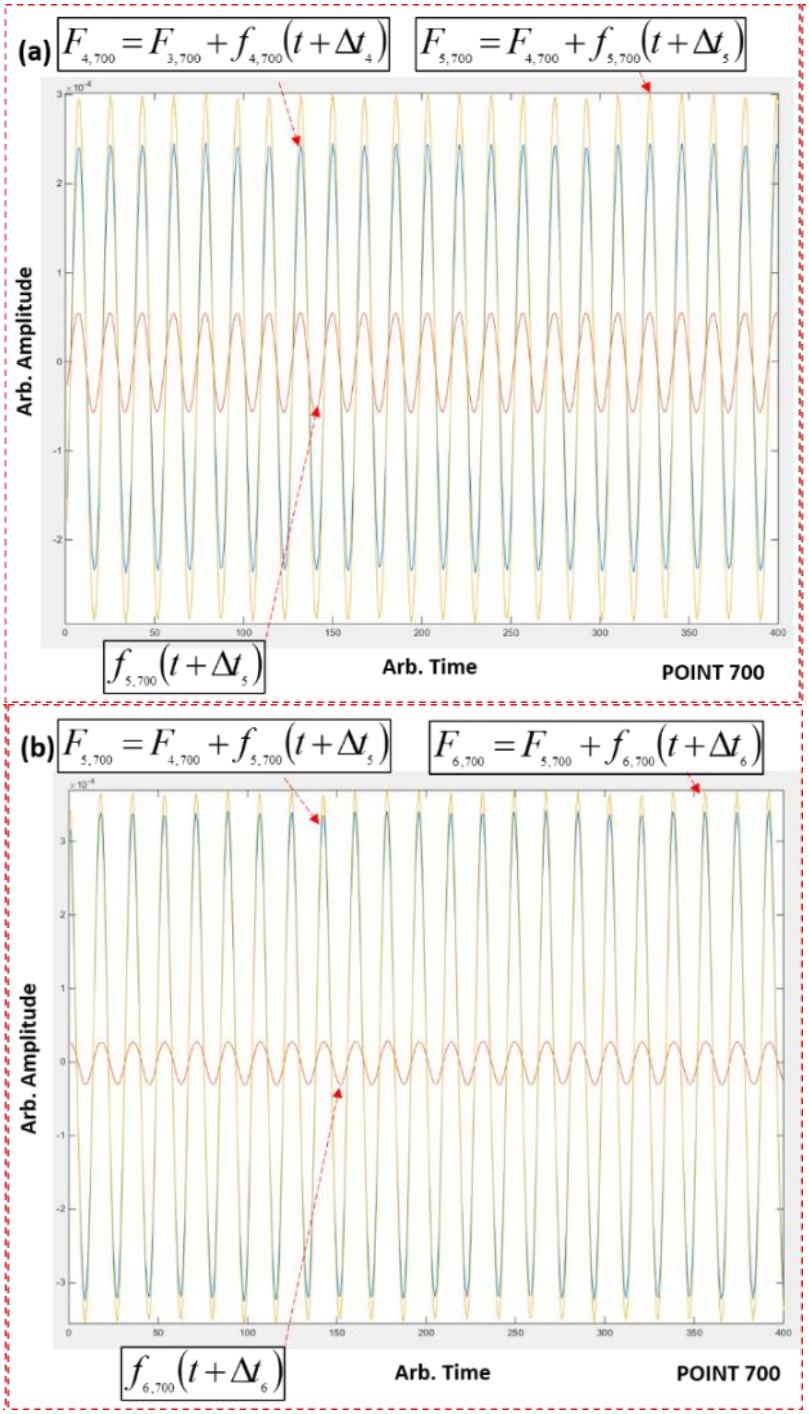

Figure 12: CNA Technique Breakdown for (a) five (P=5) and (b) six (P=6) transmit positions

5. Results and Discussion

5.1. Individual location excitation

The frequency responses for all grid points were evaluated for the six transmit positions tested (P=6). The results for the nonlinear parameters (equation 12) were plotted for each grid point after evaluating the raw time domain responses and an image of the nonlinear responses ($\beta, \gamma, \delta, \varepsilon, A_{Half}$) over the tested area was generated (Figure 13 to Figure 17). A robust local regression analysis was used to smooth the raw data (using MATLAB function 'rlowess'), this method is a robust procedure for reducing the influence of outliers and focuses on residual analysis in order to determine these outliers.

The results for individual j transmitting positions ($f_{1,k}(t)$ for example) are shown for each of the nonlinear parameters in Figure 13 to Figure 17. In the images a dotted red line is used to represent the position of the web of the t-section, thus damage if captured using the CNA method should fall to the right of this line.

Considering the $\beta, \gamma, \delta, \varepsilon, A_{Half}$ responses for each location j it is clear that there is generally an order of magnitude difference between the lowest and highest values for all transducer positions tested (1 to 6). Individually it can be difficult to determine damage location, for example for β (Figure 13) the response only matches the damage location when exciting from position j=1. The variability of the maximum response amplitude of β (between 0.18 to 3) and the locations of these maxima values for the different excitation positions demonstrates how sensitive transducer location can be in the damage/defects evaluation process.

These effects can be attributed to directionality and magnitude of the incident wave propagating towards the damage/defect regions and how these are affected by the composite structures geometry (wave reflections) and mechanical properties i.e. attenuation, the way the wave interacts with boundaries, changes in boundary geometry and importantly for nonlinear evaluation interaction with the damage/defects. Further complicating these factors is the generation of harmonics at damage/defect locations and propagation from these locations, which are dependent on the incident wave location and magnitude.

From the individual transducer location results it is clear that only certain locations clearly highlight the defect, these defect locations can be hidden due to equipment nonlinearities. For example if γ for j=2 is considered (Figure 14), the defect location seems to be evident to the right of the red dotted line, although the image will also suggest that there is a defect located in the bottom left region. The issue lies in distinguishing between actual defect responses and those that are unrelated. These issues of excitation location, amplitude and discerning between actual damage and spurious effects are exhibited in all the nonlinear parameters evaluated at individual positions. Results for $\delta, \varepsilon, A_{Half}$ are shown in Figure 15, Figure 16 and Figure 17.

The CNA methodology looks to reduce and alleviate spurious responses and focus on those generated by actual defect locations, this will be shown in the compiled CNA images (Figure 19 and Figure 20). The CNA images were generated after evaluating nonlinearities occurring in the constructive phase matched and summed signal; for the fundamental frequency $F_{6,k}$ (equation 12, Figure 19), and for signals matched to each harmonic (frequency selective constructive interference) shown in Figure 20.

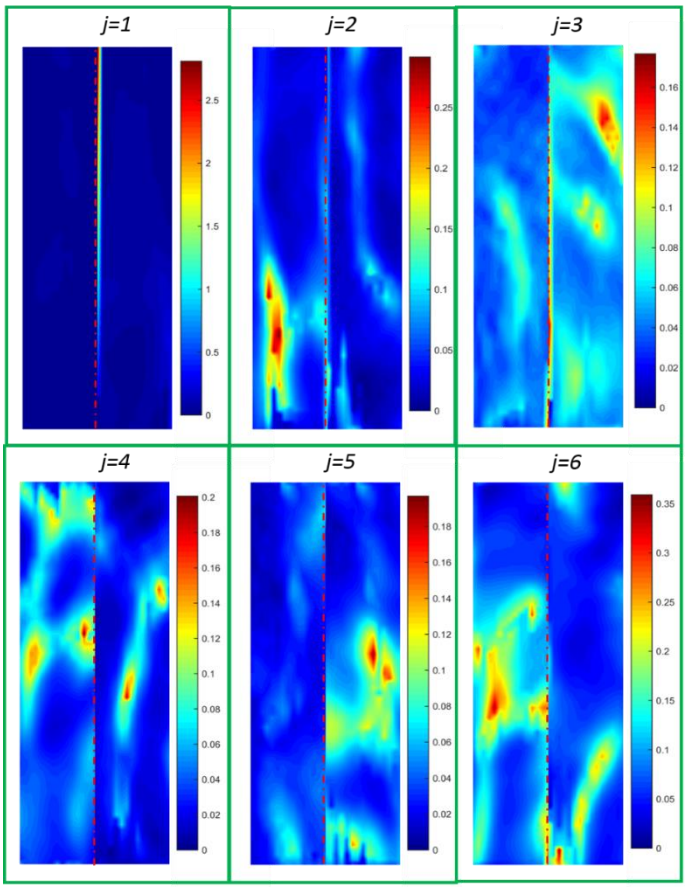

Figure 13: β response for j=1 to 6, web position separating the left and right hand LV grid points is represented by the dotted red line.

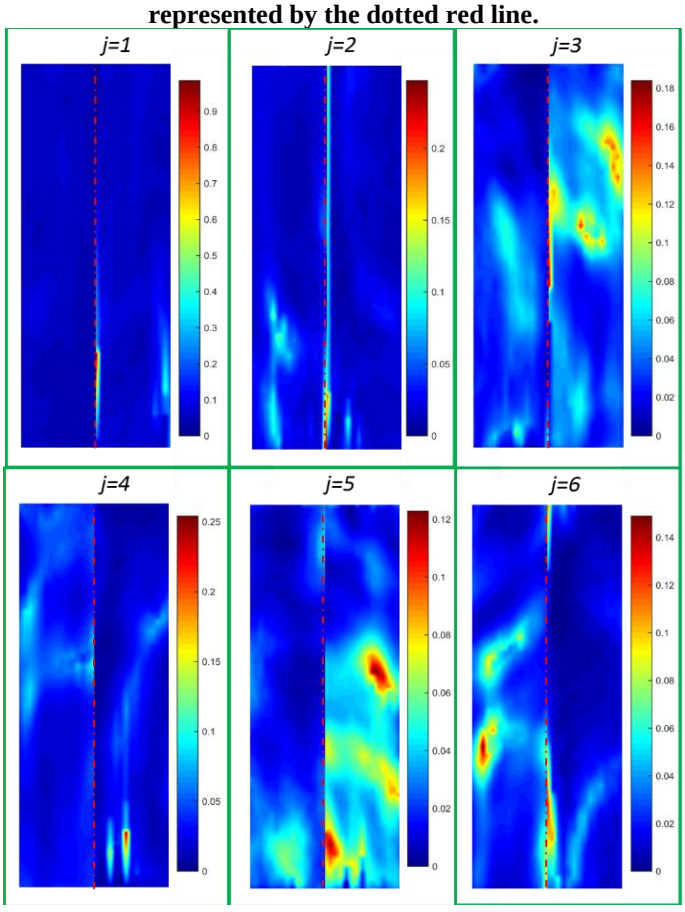

Figure 14: γ response for j=1 to 6.

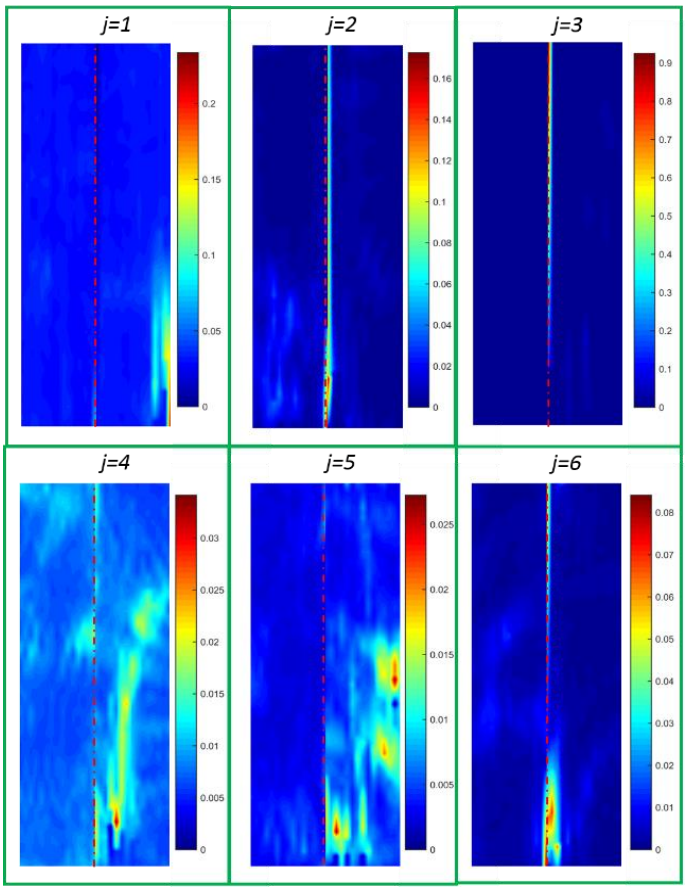

Figure 15: δ response for j=1 to 6.

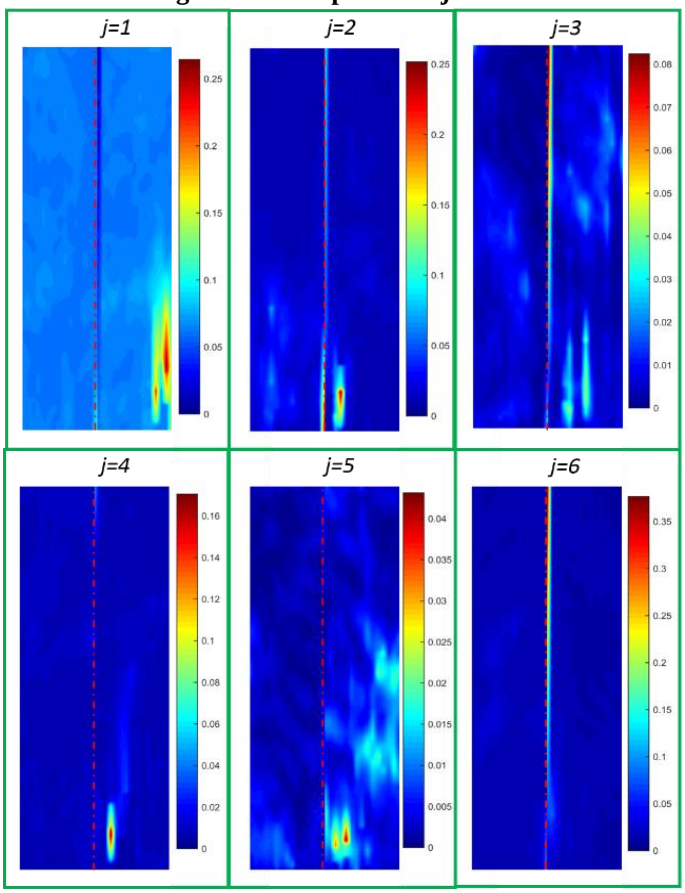

Figure 16: ε response for j=1 to 6.

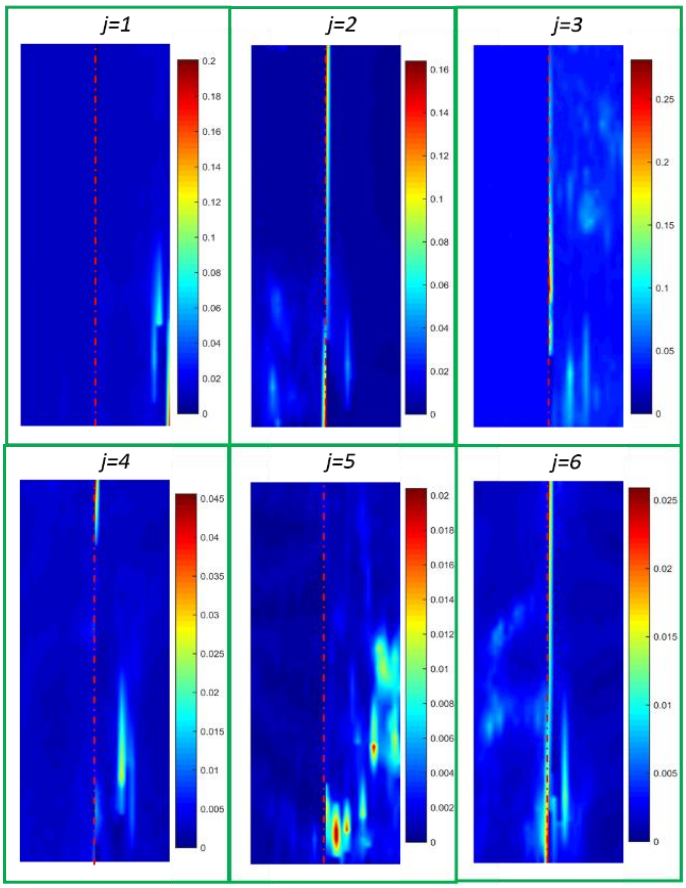

Figure 17: A_{Half} response for j=1 to 6.

5.2. CNA Evaluation

After showcasing the issues that are generally encountered when evaluating complex composite structures this section evaluates the effectiveness of the CNA methodology, looking to determine whether the hypothesised reduction in equipment nonlinearities due to attenuation is effective in locating the damage/defect. Figure 18 below shows the normalised CNA image for the fundamental harmonic response (A_1) for positions j=1 to 6. It is clear from the image that the damage location cannot be determined by evaluating the fundamental frequency response alone. But it should be noted that nonlinear ultrasound relies on a dual effect: the generation of harmonics and a reduction of the fundamental frequency response as energy is converted into these further harmonics. This increase in nonlinearities and decrease in the linear response has been shown to result in increased sensitivity in damage/defect detection.

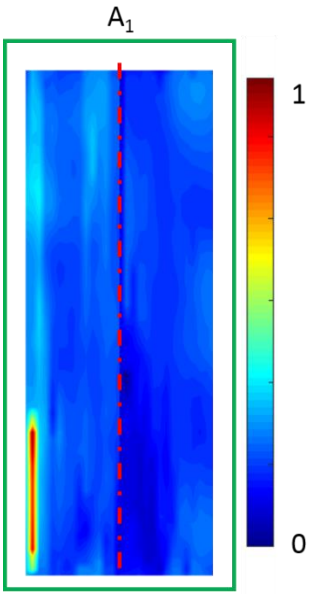

Figure 18: CNA matched to fundamental frequency response summed for positions *j=1 to 6*

Figure 19 below shows the normalised results for $\beta, \gamma, \delta, \varepsilon, A_{Half}$ when using CNA focused on matching and shifting to maximise the fundamental frequency response (as shown in Figure 12). It is evident that maxima values are more focused in the actual damage location and other areas are generally lower (cleaner) with less spurious effects. For example if A_{Half} is assessed, looking at *j*=5 (Figure 17) it would suggest that there is some damage/defect located to the middle right of the inspected area. But after CNA reconstruction these areas are significantly reduced, thus these responses can be assumed to be a direct result of exciting from that location and are not a damage/defect response. These observations are seen for the other nonlinear parameters, and suggest that the CNA methodology is working as hypothesised, reducing equipment based harmonics and focusing on actual damage generated harmonics; as was suggested in equation 23 ($\sum_{j=1}^{m} A_{h,j,k,equip} << \sum_{j=1}^{m} A_{h,j,k,dam}$).

One important factor that has not yet been discussed for CNA construction when matching to the fundamental, which is the issue of the phase of the harmonics (2 to 5 and the ½). It would be unrealistic to assume that the nonlinear phase matches that of the fundamental, therefore it is likely that there is some level of deconstructive interference between the produced harmonics when focusing on the fundamental. This means the summed signals (1 to 6) can actually result in a reduction in the amplitude of harmonics, which is further compounded by the fact that fundamentals amplitude will always increase. The solution to this issue is focusing on the individual harmonics and constructing each one individually to ensure the maximum values for $A_{1/2}$ to A_5. Thus when summation for multiple *j* position these will always result in an increase of the nonlinear parameters over the whole inspected area. Figure 20 shows the results for each nonlinear parameter when each harmonic is maximised by focusing on the respective harmonics. There is a clear increase in the contrast between the defected location and undamaged regions for β and ε, with the defect location clearer for β and γ, and the area to the bottom right of the damage region has reduced in δ and ε. In Figure 19 there is a larger nonlinear response towards the bottom of the defect when compared to Figure 20. It should be recorded, that Figure 19 is phased matched to the fundamental frequency which may results in either constructive or destructive interference of higher order harmonics contained in the raw time signal. As such, the results produced using this methodology result in inconsistent results.

In Figure 20 δ and A_{Half} still exhibit some artefacts towards the bottom right, which seem to obscure the results and suggest that they should be perceived as damage. But it should be noted that in both

these images, these artefacts have an amplitude of <30-35% of the maximum defect amplitude and thus are small comparatively. Thus providing further improvement to the results obtained using CNA matched to the fundamental.

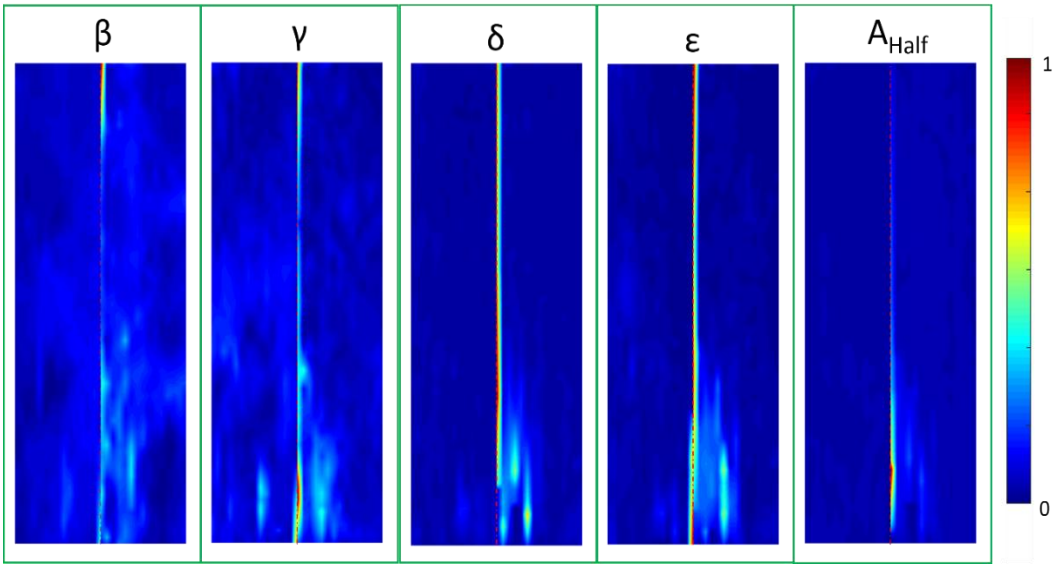

Figure 19: CNA matched to fundamental frequency response for each nonlinear parameter summed for positions *j=1 to 6*

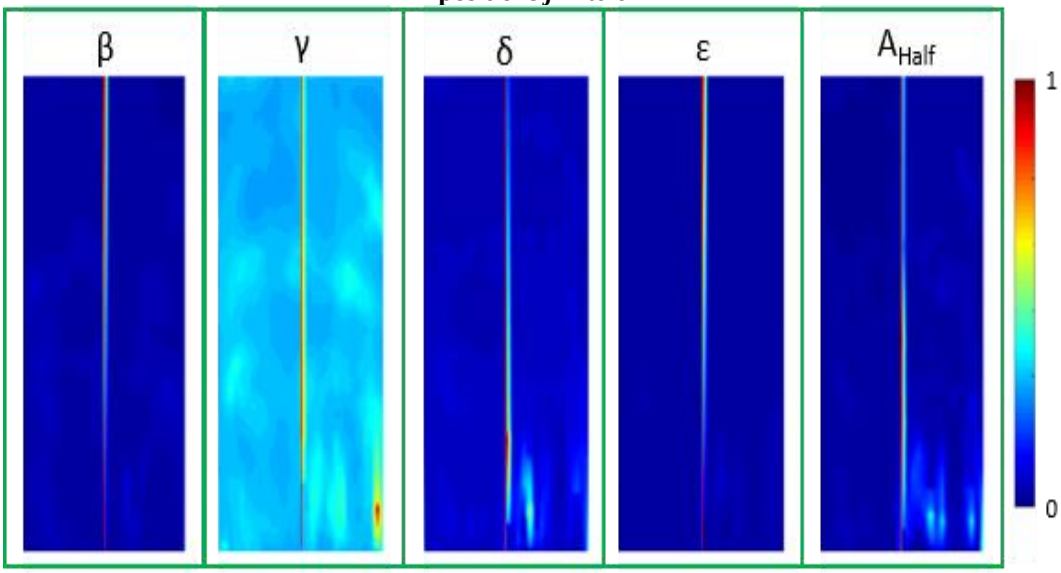

Figure 20: CNA matched to individual harmonic response for each nonlinear parameter summed for positions *j=1 to 6*

The CNA method (matched to individual harmonics) was further evaluated by assessing additional excitation positions on the evolution of the final nonlinear parameter image ($\beta,\gamma,\delta,\varepsilon,A_{Half}$), this was done by assessing the results for 2, 4 and 6 transmit positions and normalising to the maximum value according to the 6 transmit position results. Figure 21 below shows the three scenarios evaluated for each parameter, as is expected the defect location becomes more visible as transmit positions are added. The effect of each transmit position on the total image is highly dependent on its location but also on the number of transmit positions, the higher the number the less the contribution of each extra element (depicted in Figure 12).

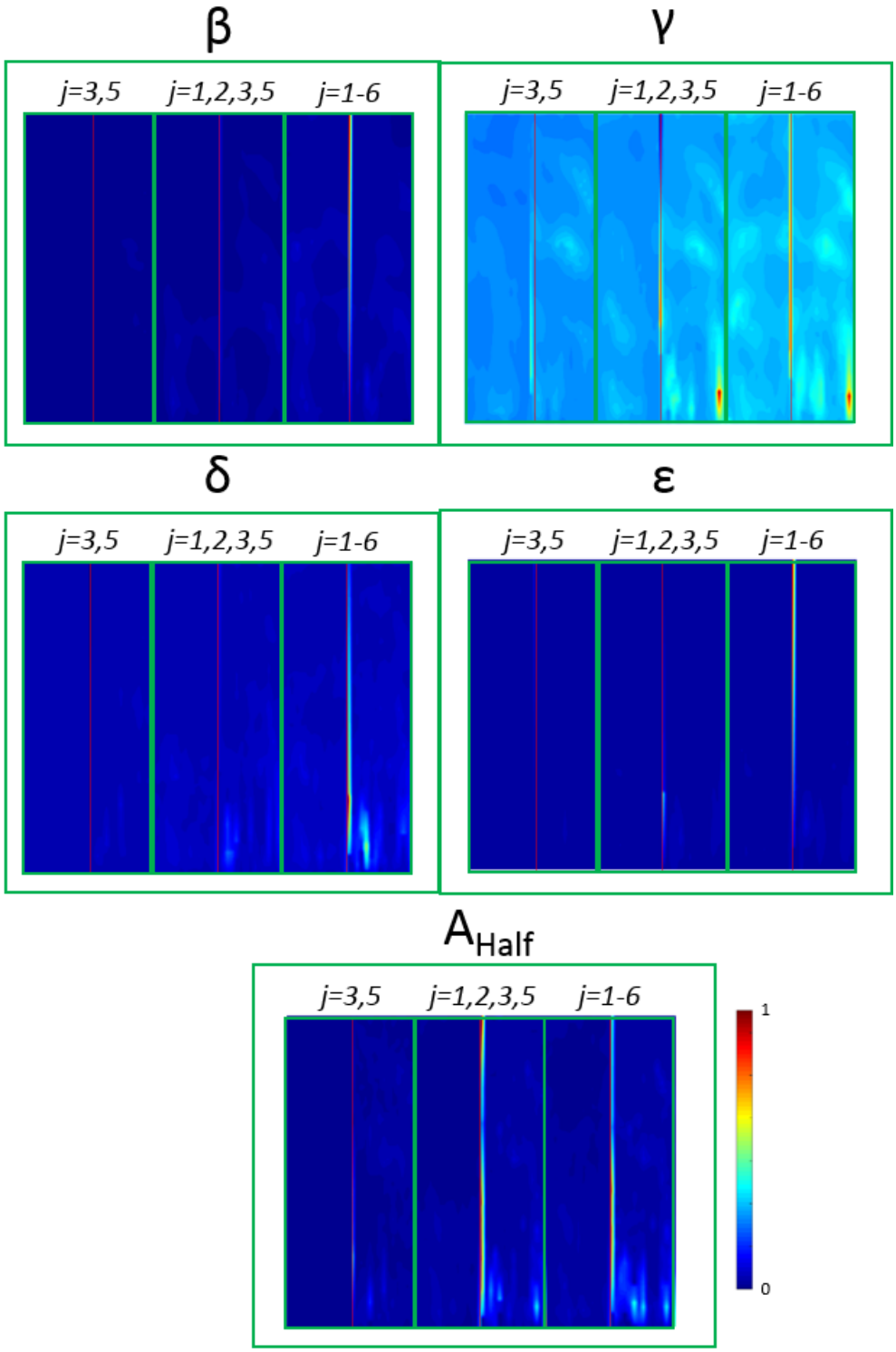

Figure 21: CNA matched to individual harmonic responses for summed positions: *j=3 and 5, j=1, 2, 3 and 5 and j=1 to 6* (left to right)

Production and propagation of damage generated nonlinearities can vary depending on a multitude of factors such as; excitation signal (amplitude and frequency) and material/damage properties. Thus in order to evaluate whether six transmit positions is sufficient for the tested sample a threshold was applied to the β results. β was used as the energy conversion from the fundamental to the second harmonic is generally the largest (refer to Figure 22). The thresholds were applied as a percentage of the max β value with anything below the threshold reduced to zero.

With the threshold set at zero, it is clear that there are some nonlinearities produced either side of the damage area, which can be assumed to be equipment generated nonlinearities (damage location is

known). A 10% level shows that most of the nonlinearities either side of the damage have disappeared. This suggests that most equipment based nonlinearities are <10% of the max damage generated nonlinearity (up to an order of magnitude greater), with all equipment based nonlinearities falling below 20%. It can be seen from Figure 21 that the damage, in most cases, only becomes visible once six transmit transducers are used. Thus four positions are not sufficient to reduce equipment based harmonics in this case, with six transmit positions regarded as the minimum requirement.

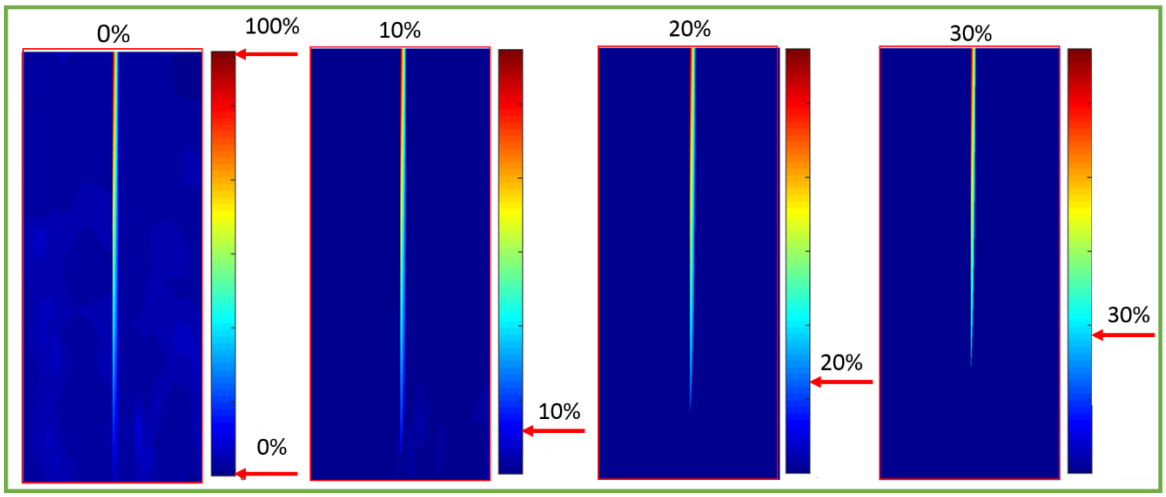

Figure 22: Threshold Analysis for β, 0%, 10%, 20% and 30%

6. Conclusion

A Constructive Nonlinear Array (CNA) technique is proposed in this paper for the detection of defects/damages in complex composite structures. This method relies on a post-process technique that phase-matches and constructively sums signals captured at multiple grid positions (k) given multiple transmitting positions (j), the results show that the method increases accuracy and repeatability of nonlinear imaging techniques (NIM). The main reason for this is the hypothesis of diminishing equipment harmonics given an array of increasing transmit positions, which has been demonstrated experimentally.

The main advantages of CNA are: (1) the location of excitation does not have to be directly above or in-line with the damage as the whole structure is vibrated, (2) due to the lower frequency excitation, larger areas can be evaluated with lower energy costs, (3) nonlinear methods have been proven to be more sensitive to smaller damages when compared with linear techniques, and (4) the reduction in equipment related issues (nonlinearities) provides a big improvement which has previously hindered nonlinear techniques. By alleviating these equipment issues found in most NIM techniques, CNA provides a step forward in terms of acceptance of NIM techniques in industry.

Further to this, the generated CNA images presented in this paper clearly demonstrate the ability of this techniques to locate defects/damage by assessing nonlinearities generated by such regions. Multiple nonlinear responses ($\beta, \gamma, \delta, \varepsilon, A_{Half}$) over the tested area were assessed, due to the constructive interference methodology proposed by this technique they yielded good results and highlighted the effectiveness of the proposed technique.

References:

[1] Chen C. Ultrasonic and advanced methods for nondestructive testing and material characterization: World Scientific Pub Co Inc; 2007.
[2] Bar-Cohen Y. In-Service NDE of Aerospace Structures–Emerging Technologies and Challenges at the end of the 2nd Millennium. NDT net. 1999;4(9):1–21.
[3] Tan K, Guo N, Wong B, Tui C. Experimental evaluation of delaminations in composite plates by the use of Lamb waves. Compos Sci Technol. 1995;53:77-84.
[4] Lemistre M, Gouyon R, Kaczmarek H, Balageas D. Damage localization in composite plates using wavelet transform processing on Lamb wave signals. Office National D Etudes Et De Recherches Aerospatiales Onera-Publications-TP1999.
[5] Meo M, Polimeno U, Zumpano G. Detecting Damage in Composite Material Using Nonlinear Elastic Wave Spectroscopy Methods. Appl Compos Mater. 2008;15:115-26.
[6] Achenbach J, Lin W, Keer L. Mathematical modelling of ultrasonic wave scattering by sub-surface cracks. Ultrasonics. 1986;24:207-15.
[7] Kim SB, Sohn H. Instantaneous reference-free crack detection based on polarization characteristics of piezoelectric materials. Smart Materials and Structures. 2007;16:2375.
[8] Krautkramer J, Krautkramer H. Ultrasonic testing of materials. Springer- Verlag New York, Inc 1977, 667 p(Book). 1977.
[9] Kundu T. Ultrasonic nondestructive evaluation: engineering and biological material characterization: CRC press; 2004.
[10] Morris W, Buck O, Inman R. Acoustic harmonic generation due to fatigue damage in high strength aluminum. J Appl Phys. 2009;50:6737-41.
[11] Hillis AJ, Neild SA, Drinkwater BW, Wilcox PD. Global crack detection using bispectral analysis. Proceedings of the Royal Society A: Mathematical, Physical and Engineering Science. 2006;462:1515.
[12] Donskoy DM, Sutin AM. Vibro-acoustic modulation nondestructive evaluation technique. J Intel Mat Syst Str. 1998;9:765.
[13] Dutta D, Sohn H, Harries KA, Rizzo P. A Nonlinear Acoustic Technique for Crack Detection in Metallic Structures. Struct Health Monit. 2009;8:573-.
[14] Jhang KY. Nonlinear ultrasonic techniques for nondestructive assessment of micro damage in material: A review. International Journal of Precision Engineering and Manufacturing. 2009;10:123-35.
[15] Solodov I, Bai J, Bekgulyan S, Busse G. A local defect resonance to enhance acoustic wave-defect interaction in ultrasonic nondestructive evaluation. Applied Physics Letters. 2011;99:211911.
[16] Solodov I, Bai J, Busse G. Resonant ultrasound spectroscopy of defects: case study of flat-bottomed holes. Journal of Applied Physics. 2013;113:223512.
[17] Solodov I. Resonant acoustic nonlinearity of defects for highly-efficient nonlinear NDE. Journal of Nondestructive Evaluation. 2014;33:252-62.
[18] Oralkan Ö, Ergun AS, Johnson JA, Karaman M, Demirci U, Kaviani K, et al. Capacitive micromachined ultrasonic transducers: Next-generation arrays for acoustic imaging? Ultrasonics, Ferroelectrics, and Frequency Control, IEEE Transactions on. 2002;49:1596-610.
[19] Chiao RY, Thomas LJ. Analytic evaluation of sampled aperture ultrasonic imaging techniques for NDE. Ultrasonics, Ferroelectrics, and Frequency Control, IEEE Transactions on. 1994;41:484-93.
[20] Holmes C, Drinkwater BW, Wilcox PD. Post-processing of the full matrix of ultrasonic transmit–receive array data for non-destructive evaluation. NDT & E International. 2005;38:701-11.
[21] Sugawara A, Jinno K, Ohara Y, Yamanaka K. Closed-crack imaging and scattering behavior analysis using confocal subharmonic phased array. Japanese Journal of Applied Physics. 2015;54:07HC8.
[22] Ohara Y, Mihara T, Sasaki R, Ogata T, Yamamoto S, Kishimoto Y, et al. Imaging of closed cracks using nonlinear response of elastic waves at subharmonic frequency. Applied physics letters. 2007;90:011902.
[23] Ohara Y, Yamamoto S, Mihara T, Yamanaka K. Ultrasonic evaluation of closed cracks using subharmonic phased array. Japanese Journal of Applied Physics. 2008;47:3908.
[24] Ohara Y, Endo H, Mihara T, Yamanaka K. Ultrasonic measurement of closed stress corrosion crack depth using subharmonic phased array. Japanese Journal of Applied Physics. 2009;48:07GD1.
[25] Ohara Y, Shintaku Y, Horinouchi S, Ikeuchi M, Yamanaka K. Enhancement of selectivity in nonlinear ultrasonic imaging of closed cracks using amplitude difference phased array. Japanese Journal of Applied Physics. 2012;51:07GB18.
[26] Ohara Y, Takahashi K, Murai S, Yamanaka K. High-selectivity imaging of closed cracks using elastic waves with thermal stress induced by global preheating and local cooling. Applied Physics Letters. 2013;103:031917.
[27] Potter J, Croxford A, Wilcox P. Nonlinear ultrasonic phased array imaging. Physical review letters. 2014;113:144301.

[28] Park C-S, Kim J-W, Cho S, Seo D-c. A high resolution approach for nonlinear sub-harmonic imaging. NDT & E International. 2016;79:114-22.
[29] Chatillon S, Cattiaux G, Serre M, Roy O. Ultrasonic non-destructive testing of pieces of complex geometry with a flexible phased array transducer. Ultrasonics. 2000;38:131-4.
[30] Chatillon S, De Roumilly L, Porre J, Poidevin C, Calmon P. Simulation and data reconstruction for NDT phased array techniques. Ultrasonics. 2006;44:e951-e5.
[31] Haiat G, Lhémery A, Calmon P, Lasserre F. A model-based inverse method for positioning scatterers in a cladded component inspected by ultrasonic waves. Ultrasonics. 2005;43:619-28.
[32] Casula O, Poidevin C, Cattiaux G, Dumas P. Control of complex components with smart flexible phased arrays. Ultrasonics. 2006;44:e647-e51.
[33] Xu N, Zhou Z. Numerical simulation and experiment for inspection of corner-shaped components using ultrasonic phased array. NDT & E International. 2014;63:28-34.
[34] Bowen C, Bradley L, Almond D, Wilcox P. Flexible piezoelectric transducer for ultrasonic inspection of non-planar components. Ultrasonics. 2008;48:367-75.
[35] Ciampa F, Meo M. Nonlinear elastic imaging using reciprocal time reversal and third order symmetry analysis. The Journal of the Acoustical Society of America. 2012;131:4316-23.
[36] Fierro GM, Ciampa F, Ginzburg D, Onder E, Meo M. Nonlinear ultrasound modelling and validation of fatigue damage. Journal of Sound and Vibration. 2015;343:121-30.
[37] Landau L, Lifshitz E, Sykes J, Reid W, Dill EH. Theory of Elasticity: Vol. 7 of Course of Theoretical Physics. Physics Today. 1960;13:44.
[38] Meo M, Zumpano G, Piggott M, Marengo G. Impact identification on a sandwich plate from wave propagation responses. Composite Structures. 2005;71:302-6.
[39] Zumpano G, Meo M. Damage localization using transient non-linear elastic wave spectroscopy on composite structures. Int J Nonlin Mech. 2008;43:217-30.
[40] Fierro GPM, Meo M. Residual fatigue life estimation using a nonlinear ultrasound modulation method. Smart Materials and Structures. 2015;24:025040.
[41] Korshak B, Solodov IY, Ballad E. DC effects, sub-harmonics, stochasticity and “memory” for contact acoustic non-linearity. Ultrasonics. 2002;40:707-13.
[42] Ohara Y, Mihara T, Yamanaka K. Effect of adhesion force between crack planes on subharmonic and DC responses in nonlinear ultrasound. Ultrasonics. 2006;44:194-9.
[43] Jhang K-Y. Nonlinear ultrasonic techniques for nondestructive assessment of micro damage in material: a review. International journal of precision engineering and manufacturing. 2009;10:123-35.
[44] Cantrell JH. Fundamentals and applications of non-linear ultrasonic nondestructive evaluation. Ultrasonic non-destructive evaluation. 2004;vol. 6:p.363-434.
[45] Meo M, Amerini F, Amura M. Baseline-free estimation of residual fatigue life using third order acoustic nonlinear parameter. The Journal of the Acoustical Society of America 2010;4:1829-37.